

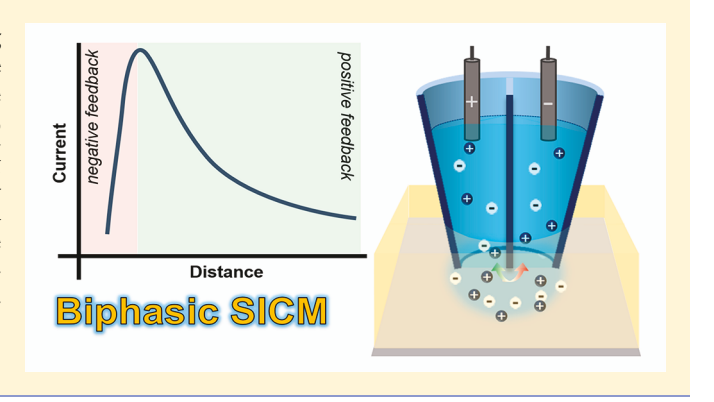
Biphasic-Scanning Ion Conductance Microscopy

Myunghoon Choi and Lane A. Baker*

Department of Chemistry, Indiana University, 800 E. Kirkwood Avenue, Bloomington, Indiana 47405, United States

Supporting Information

ABSTRACT: A concentration gradient driven imaging mechanism is described for scanning ion conductance microscopy (SICM). Two different solution phases, one filling a double-barrel pipet and one in the bath, are used to afford probe control and imaging under nonstandard SICM conditions. Under these conditions, solutions with no added electrolyte can be utilized as the bath solution. Further, both positive and negative feedback modes are exhibited as the probe approaches the surface. We term this method biphasic-SICM (BP-SICM). Technical details of implementing BP-SICM and operational principles are described herein.



 \mathbb{C} canning ion conductance microscopy $(SICM)^1$ provides noninvasive topographic imaging in electrolyte solutions with high resolution and has been extensively utilized for in situ imaging of biomaterials,² cell membranes,^{3,4} living cells,⁵ and tissues.9 SICM has also found application to characterization beyond imaging, for instance, measurement of surface charge at interfaces, ^{2,10,11} mapping mechanical stiffness of cell membranes, 12 and localized electrochemical measurements. 13 Dual-barrel SICM platforms, where two barrels are colocated at the same pipet tip, have proven very useful for advanced SICM techniques. For instance, Korchev and co-workers demonstrated dispensation of water droplets at surfaces with dual-barrel nanopipettes in organic solvents. 14 Dual-barrel pipettes have also proven especially useful for techniques with complementary electrochemical imaging techniques, as demonstrated clearly by scanning electrochemical cell microscopy (SECCM) which affords versatile, high-resolution electrochemical measurement. $^{15-17}$

In a recent report, Unwin and co-workers described differential concentration SICM (Δ C-SICM), ¹⁰ which employs a single-barrel SICM platform for enhanced SICM measurements and uses concentration gradient driven ion currents with small applied electric potentials. Here, we describe a complementary concentration gradient driven approach to SICM that uses dual-barrel probes. The method is applicable to multiphase systems where the pipet is filled with one liquid phase and the solution surrounding the pipet (bath solution) consists of a second phase; thus, we term the method biphasic-scanning ion conductance microscopy (BP-SICM).

The feedback for BP-SICM and image acquisition parameters are significantly different than typical SICM, which provides advantages for unique applications. First, atypical electrolytes may be chosen for the bath solution, including nonaqueous solvents or solvents with little or no

(intended) electrolyte. Second, under proper conditions (e.g., positive feedback and appropriate concentration gradients between the pipet solution and bath solution), BP-SICM affords operation at longer working distances, but with good topographic resolution, which can prove beneficial for noncontact imaging. Further, as demonstrated here, the working distance and feedback (positive or negative) can be chosen as desired. Third, new realms of electrolyte composition can be interrogated with SICM, which provides access to new fundamental studies. Here, we describe the operation, current—distance relationship, and imaging principles for BP-SICM. Results obtained are compared to atomic force microscopy (AFM) images of collagen fibrils.

EXPERIMENTAL SECTION

Solutions and Materials. Aqueous electrolyte solutions (0.1 M KCl and 1.0 M KCl) were prepared with deionized water (DI $\rm H_2O$, resistivity ca. 18 M $\rm \Omega$ -cm at 25 °C, Millipore Corp., Danvers, MA, USA). For selected experiments, absolute ethanol (Greenfield Global, Toronto, Canada) was used as a bath solution. Hydrochloric acid (EMD Millipore corp., Darmstadt, Germany) was used to prepare solutions for pH studies. Elastomer substrates used for imaging were prepared as described in the Supporting Information.

Nanopipette Fabrication. Pipettes were pulled with a $\rm CO_2$ -laser puller (P-2000, Sutter Instrument, Novato, CA, USA) from theta or single quartz capillaries (QT120-90-7.5 or Q100-70-7.5, Sutter Instrument, Novato, CA, USA). Pulling parameters for theta were as follows: Heat = 690/690, Fil = 3/4, Vel = 35/45, Del = 160/160, and Pull = 160/190. Pipettes were characterized by electron microscopy (FEI Quanta-FEG,

Received: August 12, 2018
Accepted: September 20, 2018
Published: September 20, 2018



Hillsboro, OR, USA) with outer diameters of dual-barrel pipettes estimated to be 120–230 nm (Figure S1). Pipettes were filled with potassium chloride (KCl) solution, and Ag/AgCl electrodes were inserted into each dual barrel as quasi-reference counter electrodes (QRCEs). For dual barrel applications, one electrode served as a working electrode and the second electrode, as a counter/quasi-reference electrode. To minimize crosstalk between barrels, Ag/AgCl electrodes were prepared from perfluoroalkoxy (PFA) coated silver wire (0.005 in. bare, 0.007 in. coated, A-M Systems, Sequim, WA, USA) with the ends stripped to expose silver, which was subsequently chloridized.

BP-SICM Instrumentation. A modified XE-Bio (Park systems, Suwon, South Korea) SICM was used to control pipet position and record electrochemical signals. In experiments described here, both positive and negative feedback were employed, with standard hardware/software. To enable positive feedback with the negative feedback algorithm from the commercial instrument, the current signal (voltage) was passed through a voltage inverter and to the feedback input. With BP-SICM, probe control was achieved with DC (direct current), AC (or distance modulated), and ARS (approachretract scan, or "hopping") modes, with the imaging set points optimized dependent on the peak current (i_p) value (described vide infra). (Further details of imaging parameters for AC mode are included in Supporting Information.) For probesurface distance (Dps) estimations, the point of closest approach was set as zero, as the complex concentration gradients make standard SICM equations invalid. To evaluate and compare the resolution of BP-SICM, topography of collagen fibrils was also measured with atomic force microscopy (AFM, XE-Bio, Park systems, Suwon, South Korea). Biolever-mini cantilever (BL-AC40TS, Olympus, Tokyo, Japan) and tapping mode imaging were used for both aqueous and ambient conditions.

■ RESULTS AND DISCUSSION

Biphasic Operations and Measurement. The general experimental configuration employed here is shown in Figure 1. A dual-barrel pipet is filled with electrolyte solution (e.g., 1 M KCl), and reference electrodes are inserted in each barrel. A potential is applied to the electrode of one barrel, and the electrode in the second barrel serves as ground. Current flows between the electrodes in the two barrels, similar to the situation for SECCM¹⁶ and previous studies of Korchev and co-workers.14 In configurations described here, a lower concentration electrolyte (or no electrolyte) was present in the bath solution, and as such, in addition to an ion current due to migration under the applied potential difference, ions also diffuse from each barrel to the surrounding solution under a concentration gradient. As long as the ions are miscible in the bath solution, this creates a local zone of ion concentration at the tip of the pipet suitable for generating feedback and probe control in imaging, as described below.

The dual-barrel tip and concentration gradient in BP-SICM generate a unique approach curve profile relative to typical SICM measurements. Generally, approach curves for BP-SICM are characterized as initially showing a current increase, followed by a peak current (i_p) and subsequent decrease in current, as shown schematically in Figure 1b and experimentally for approach to a PDMS surface (Figure 2a,b). The initial increase in current happens at distances relatively far (>300 nm) in comparison to standard SICM. For this

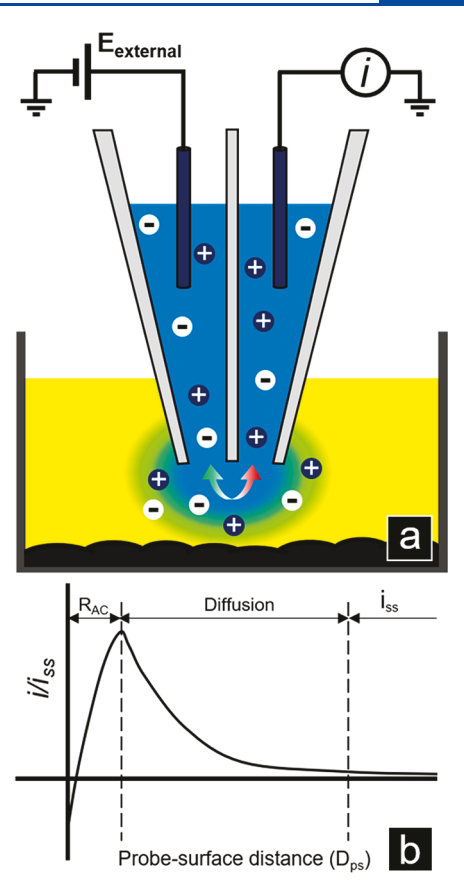


Figure 1. Schematic of (a) biphasic-SICM (BP-SICM) setup depicting different electrolyte phases in the pipet and bath solution; (b) schematic of the BP-SICM approach curve relative to diffusional current increases and access resistance ($R_{\rm AC}$) of SICM.

increasing region of the approach curve, the current increase occurs as the diffusional space under the probe tip narrows on approach, limiting the volume of solution into which ions immediately diffuse and effectively increasing the local concentration of ions (i.e., conductivity). Under conditions here, typical current increases were approximately 10-20% of the steady state current (i_{ss}) , values more than suitable to generate feedback. Eventually, the local concentration reaches a maximum, observed as a peak current (i_p) , and then, geometric factors of the access resistance (R_{AC}) , surface, and probe geometry result in a current decrease, similar to the case for typical SICM. The maximum current (the peak current, i_p) is proportional to the applied electric potential (E_{external}) . After reaching the i_p , the current decreases dramatically below the i_{ss} value, similar to what is encountered for traditional feedback generated from RAC as the tip moves toward the surface. Approach curves at positive and negative potentials and in the presence of 0.1 M HCl (Figure S2) showed the same general trend in the approach curve prior to i_p , which supports the diffusional origin of feedback proposed, as opposed to influences arising from surface charges. From approach curves at positive and negative potentials, we can observe that concentration polarization results in different magnitudes in the presence of surface charge. Generally, for BP-SICM measurements without added acid, the symmetric nature of the dual barrel probe, far working distances, and high electrolyte concentration in the pipet mitigate significant effects from surface charge.

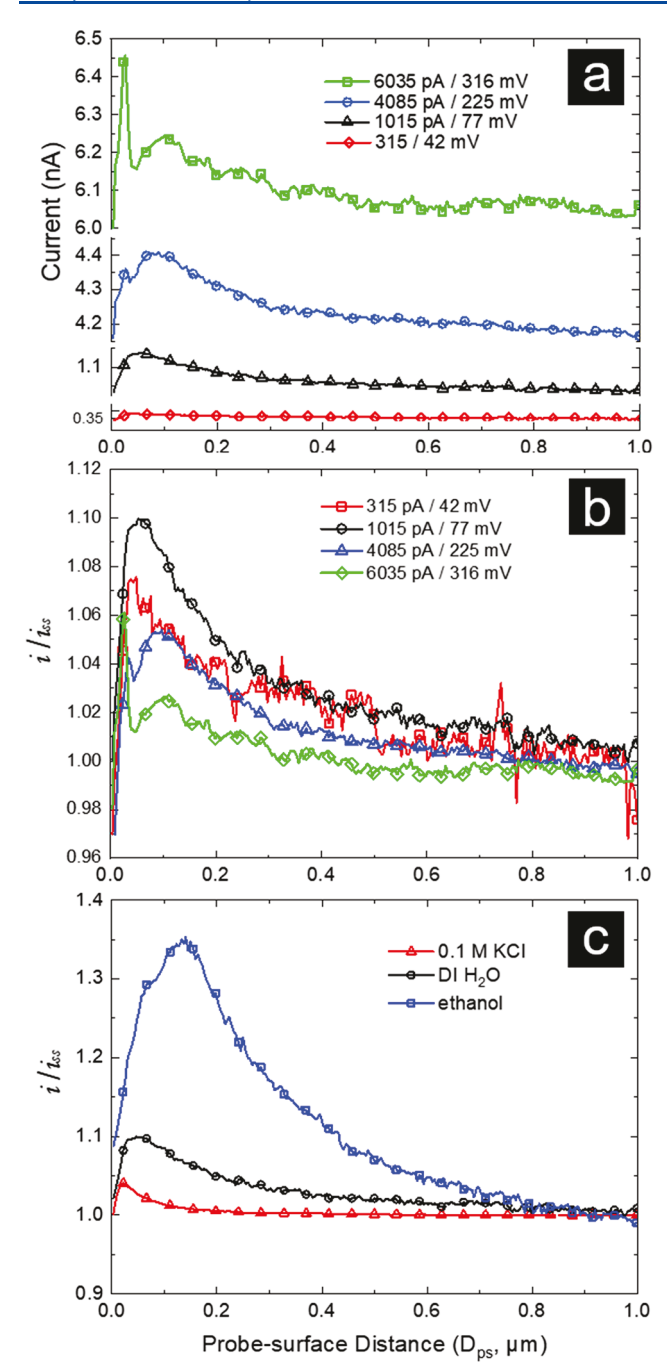


Figure 2. Experimental approach curves of BP-SICM. (a) Effect of applied potential difference on current—distance relationship. (b) Normalized approach curves collected at each applied potential. (c) Approach curves collected with different bath solvents/solutions on flat PDMS substrate. The steady state current (i_{ss}) and externally applied electric potentials (E_{external}) were as follows for the bath solution: 0.1 M KCl, 1069 pA/49 mV (red \triangle); DI H₂O, 1015 pA/57 mV (black O); ethanol, 1118 pA/8.8 V (blue □).The pipettes were filled with 1.0 M KCl for each instance.

BP-SICM can also operate in what would typically be considered an unconventional solvent for SICM, with the only requirement being solubility of ions in the electrolyte in the external bath solution. We demonstrate this by collecting approach curves (Figure 2c) with 0.1 M KCl, DI $\rm H_2O$, and ethanol serving as bath solution. Under these conditions, approach curves are dependent on the electrolyte solubility.

For instance, ethanol, with a lower dielectric constant and limited KCl solubility, required high voltages (>1 V) to generate current suitable for operation.

The feedback mechanism described above proved sufficient to acquire images for configurations with 1.0 M KCl inside the pipet and lower concentrations of KCl (e.g., 0.1 M), deionized water (DI $\rm H_2O$) with no electrolyte, and nonaqueous solvents (e.g., ethanol) in the bath. Example images acquired in the DI water and ethanol are shown in Figure 3. In particular, AC

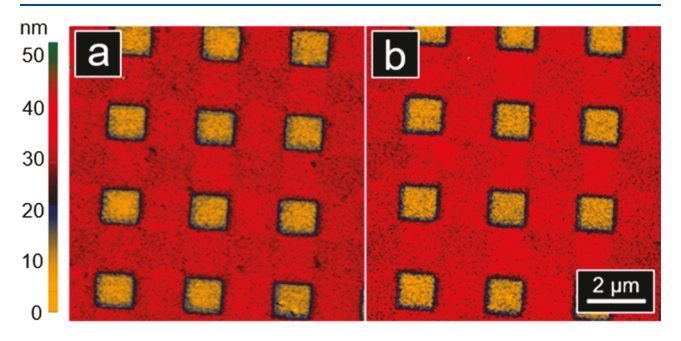


Figure 3. Topography of PDMS calibration standard replica, measured with AC mode of BP-SICM (a) in deionized water and (b) ethanol. Pipettes used were filled with 1.0 M KCl. The scale bar for (a) is same as for (b).

feedback was found to be especially useful for imaging. This is because the absolute value of the current change used for AC feedback afforded probe control regardless of if the current increased or decreased. Thus, suitable feedback at far distances, where diffusion resulted in increased ion current, or feedback at short distances, where R_{AC} resulted in decreased ion current, could be achieved. (Representative approach curves highlighting subtleties of the AC feedback signal are shown in Figure S3.) For such images, topography in nonionic solutions were readily acquired, but the roughness of the calibration standard replica in the topography was increased slightly, a consequence of the increase of noise and possibly also due to swelling in nonaqueous solutions. Image analysis (Figure S4), determining the width and height of the calibration standard replica topography for DI H₂O (bath solution), was comparable to images acquired in 0.1 M KCl. In ethanol, swelling of the PDMS substrate resulted in subtle changes in the width of calibration standard replica of 20-100 nm and nominal height increases (~1.8 nm). These changes agree well with the reported swelling ratio for PDMS in ethanol of 1.04. 18 Resolution and imaging parameters were investigated for BP-SICM in ARS mode for both positive feedback (Dps greater than i_p on the approach curve) and negative feedback (Dps less than $\hat{i_p}$ on the approach curve) and compared to AFM images of the same features in topographic images of collagen fibril bundles (Figures 4 and 5). As BP-SICM operated in the positive feedback regime (BP-SICM_{PF}) affords the opportunity to image at extended distances, optimal imaging parameters for different set points were also examined. At thresholds typical of ARS mode (1–2% of i_{ss}) in conventional SICM (single-barrel nanopipette), BP-SICM_{PF} images of collagen fibrils were poorly resolved, likely due to the extended working distances of BP-SICM. At thresholds of 7% of i_{ss} , features on collagen fibrils came into focus, with thresholds of 14% and 21% of i_{ss} allowing resolution of detailed fibril features (Figure 4). This same phenomenon was also observed for DC mode imaging with BP-SICM_{PF} (data not shown).

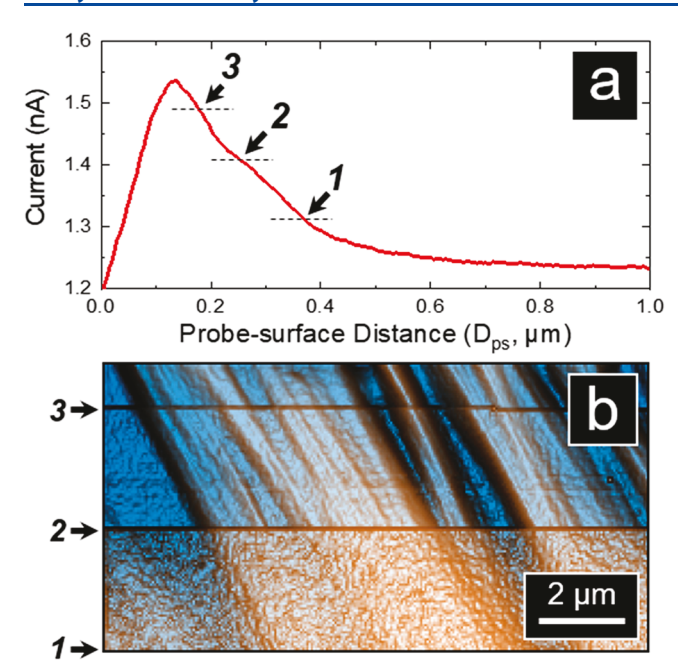


Figure 4. (a) Approach curve and (b) topography of image collection with BP-SICM_{PF} of collagen fibrils with ARS (hopping) mode in deionized water. Points denoted indicate change in ARS thresholds, where (1) = 7.0%, (2) = 14.0%, and (3) = 21.0%. Pipettes used were filled with 1.0 M KCl.

To further evaluate resolution of BP-SICM_{PF}, the same single collagen fibril was imaged by using both positive and negative feedback of BP-SICM and both in situ and ambient AFM (Figure 5). In BP-SICM_{PF}, the threshold for ARS (hopping) mode was set as 7% to secure the long working distance. In the negative feedback regime of BP-SICM (BP-SICM_{NF}), the threshold was set as 0.9%. In these image comparisons, the lateral resolution of BP-SICM_{PF} appeared as the lowest among all, showing the full width half max (fwhm) of single collagen fibrils of 600 nm (threshold 7%), as compared to 250 nm for BP-SICM_{NF}, 320 nm for in situ AFM, and 420 nm for ambient AFM. For negative feedback regimes BP-SICM_{NF} (<100 nm), D_{ps} is smaller than for BP-SICM_{PF}, which probably results in higher lateral resolution for BP-SICM_{NF}, as found that a closer working distance plays an important role in image resolution for SICM in the literature. ^{19–21} The height of the collagen topography, measured with BP-SICM_{PF}, was ~197 nm, similar to that measured by in situ/ambient AFM (190 nm/170 nm, respectively). Height measured in BP-SICM_{NF} was ~360 nm, comparable to the value recorded for the other feedback modes tested. In previous studies, SICM has consistently reported higher apparent heights observed relative to AFM measurements, presumably a result of tip-sample forces applied in tapping mode AFM, which resulted in height information measured by AFM being underestimated in the range of 30-50%. 9,22 For measurements recorded here with SICM, BP-SICM_{PF} was not as accurate as BP-SICM_{NF}, a result of the differences in D_{ps} for different feedback regimes.

CONCLUSIONS

We have reported BP-SICM, which exhibits ion current independent of bulk electrolyte composition and imaging environment. Through BP-SICM imaging and analysis, we have demonstrated topographic imaging in electrolyte free and

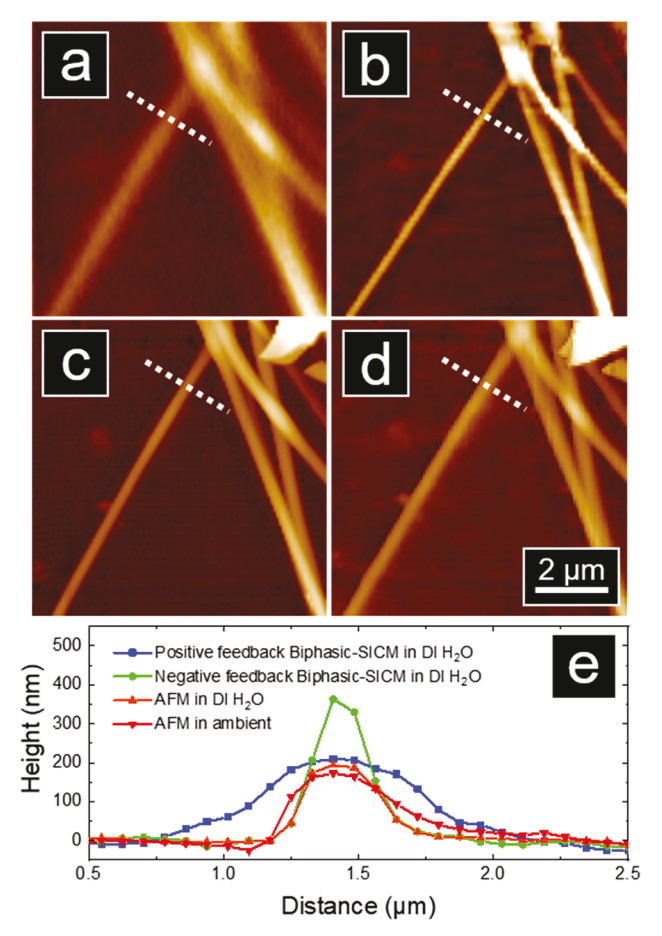


Figure 5. Topography comparison of (a) positive feedback BP-SICM_{PF} (ARS mode) in DI H₂O (blue ■), (b) negative feedback BP-SICM_{NF} (ARS mode) in DI H₂O (green ●), (c) AFM (tapping mode) in DI H₂O (orange ▲), and (d) AFM (tapping mode) in ambient (red ▼). The height and width of collagen fibril in topography are (a) 197 nm/600 nm, (b) 360 nm/250 nm, (c) 190 nm/320 nm, and (d) 170 nm/420 nm. Pipettes used were filled with 1.0 M KCl.

nonaqueous bath solutions. BP-SICM has interesting potential applications in imaging, where longer working distances may be useful in minimizing probe contamination and sample damage from the unintended physical contact for samples with extreme topography. BP-SICM also provides a simple way to image in nonaqueous solutions with minor modification of conventional SICM equipment.

ASSOCIATED CONTENT

Supporting Information

The Supporting Information is available free of charge on the ACS Publications website at DOI: 10.1021/acs.analchem.8b03660.

Experimental summary of parameters used for images collected in Figures 3 and 5; materials and methods; scanning electron micrograph; approach-curve comparison at positive and negative applied potential with normalized current value; AC feedback working principle for BP-SICM; calibration standard replica topography dimension analysis; image analysis of topography recorded for elastomer grating replica substrate; image analysis of topography of PDMS replica grating substrate (PDF)

AUTHOR INFORMATION

Corresponding Author

*Phone: (812) 856-1873. Fax: (812) 856-8300. E-mail: lanbaker@indiana.edu.

ORCID ®

Lane A. Baker: 0000-0001-5127-507X

Notes

The authors declare no competing financial interest.

ACKNOWLEDGMENTS

We acknowledge Park Systems for access to the XE-Bio (SICM/AFM) instrument. Assistance from the Electronic Instrument Service (EIS) group at Indiana University is acknowledged. We thank Prof. Tatsuo Ushiki, Niigata University, for providing collagen samples examined here. This work was supported by the National Science Foundation (CHE-1507341).

REFERENCES

- (1) Hansma, P. K.; Drake, B.; Marti, O.; Gould, S. A. C.; Prater, C. B. Science 1989, 243, 641–643.
- (2) Klausen, L. H.; Fuhs, T.; Dong, M. D. Nat. Commun. 2016, 7, 12447.
- (3) Shevchuk, A. I.; Frolenkov, G. I.; Sanchez, D.; James, P. S.; Freedman, N.; Lab, M. J.; Jones, R.; Klenerman, D.; Korchev, Y. E. Angew. Chem., Int. Ed. 2006, 45, 2212–2216.
- (4) Mizutani, Y.; Choi, M. H.; Cho, S. J.; Okajima, T. Appl. Phys. Lett. 2013, 102, 173703.
- (5) Novak, P.; Li, C.; Shevchuk, A. I.; Stepanyan, R.; Caldwell, M.; Hughes, S.; Smart, T. G.; Gorelik, J.; Ostanin, V. P.; Lab, M. J.; Moss, G. W. J.; Frolenkov, G. I.; Klenerman, D.; Korchev, Y. E. *Nat. Methods* **2009**, *6*, 279–281.
- (6) Zhu, C.; Shi, W.; Daleke, D. L.; Baker, L. A. Analyst 2018, 143, 1087–1093.
- (7) Page, A.; Kang, M.; Armitstead, A.; Perry, D.; Unwin, P. R. Anal. Chem. 2017, 89, 3021–3028.
- (8) Nakajima, M.; Mizutani, Y.; Iwata, F.; Ushiki, T. Semin. Cell Dev. Biol. 2018, 73, 125-131.
- (9) Ushiki, T.; Nakajima, M.; Choi, M.; Cho, S. J.; Iwata, F. *Micron* **2012**, 43, 1390–1398.
- (10) Perry, D.; Page, A.; Chen, B. P.; Frenguelli, B. G.; Unwin, P. R. Anal. Chem. **2017**, *89*, 12458–12465.
- (11) Zhu, C.; Zhou, L.; Choi, M.; Baker, L. A. ChemElectroChem **2018**, 5, 1-6.
- (12) Rheinlaender, J.; Schaffer, T. E. Soft Matter 2013, 9, 3230–3236.
- (13) Bentley, C. L.; Kang, M.; Unwin, P. R. J. Am. Chem. Soc. 2017, 139, 16813–16821.
- (14) Rodolfa, K. T.; Bruckbauer, A.; Zhou, D.; Schevchuk, A. I.; Korchev, Y.; Klenerman, D. J. *Nano Lett.* **2006**, *6* (2), 252–257.
- (15) Ebejer, N.; Schnippering, M.; Colburn, A. W.; Edwards, M. A.; Unwin, P. R. *Anal. Chem.* **2010**, 82, 9141–9145.
- (16) Snowden, M. E.; Guell, A. G.; Lai, S. C. S.; McKelvey, K.; Ebejer, N.; O'Connell, M. A.; Colburn, A. W.; Unwin, P. R. *Anal. Chem.* **2012**, *84*, 2483–2491.
- (17) Ebejer, N.; Guell, A. G.; Lai, S. C. S.; McKelvey, K.; Snowden, M. E.; Unwin, P. R. *Annu. Rev. Anal. Chem.* **2013**, *6*, 329–351.
- (18) Lee, J. N.; Park, C.; Whitesides, G. M. Anal. Chem. 2003, 75, 6544-6554.
- (19) Korchev, Y. E.; Milovanovic, M.; Bashford, C. L.; Bennett, D. C.; Sviderskaya, E. V.; Vodyanoy, I.; Lab, M. J. *J. Microsc.* **1997**, *188*, 17–23.
- (20) Rheinlaender, J.; Schäffer, T. E. J. Appl. Phys. 2009, 105, 094905.
- (21) Weber, A. E.; Baker, L. A. J. Electrochem. Soc. **2014**, 161, H924–H929.

(22) Kim, J.; Choi, M.; Jung, G.-E.; Ferhan, A. R.; Cho, N. J.; Cho, S. J. *Ipn. J. Appl. Phys.* **2016**, *55*, 08NB8.